HYBRID MODELING OF A TWO-STAGE TURBOCHARGED DIESEL ENGINE AIR SYSTEM

P. Kotman[1,2], M. Bitzer[1], K. Graichen[2], A. Kugi[2]
[1]Robert Bosch GmbH, Germany, [2]Vienna University of Technology, Austria

Corresponding author: P. Kotman, Corporate Sector Research and Advance Engineering, Robert Bosch GmbH, Robert-Bosch-Straße 2, 71701 Schwieberdingen, Germany, philipp.kotman@de.bosch.com

Abstract. Contemporary diesel engines are often equipped with a turbocharger to simultaneously increase their power and fuel efficiency. In order to meet tightened legal restrictions, future engines will have to feature further improved fuel consumption and pollutant emissions. Two means of achieving these goals are the use of multiple turbochargers on the one hand and exhaust-gas recirculation (EGR) on the other hand. The restriction of EGR and turbocharger usage to certain constraints (e.g. engine speed and load) results in a partitioning of the engine's region of operation into respective subsets. Consequently, an appropriate engine control scheme has to respect the resulting switching behavior of the engine's air system. A hybrid dynamical model of a state-of-the-art diesel engine air system serving for model-based control design is presented in this work. Therefore, physical models of the respective components are derived and the switching events occurring during engine operation are discussed. A simulation study concludes this paper.

1 Introduction

Today, combustion engine systems usually ought to meet different, partly conflicting requirements. On the one hand, consumers demand high power and economy, while on the other hand legislators mainly stipulate low pollutant emissions. Usually, an isolated reduction of the pollutant emissions decreases engine power and in contrast, increasing the engine's power typically raises pollutant emissions. However, an improved engine efficiency achieves both, increased power and reduced pollutant emissions. A prevalent means of increasing a combustion engine's efficiency are exhaust-driven turbochargers, consisting of a turbine situated in the engine's exhaust path, a compressor located in the fresh-air path, and a connecting shaft. The basic idea is to boost the pressure at the intake of the engine and thereby increase its power using the energy stored in the hot exhaust mass flow. As a consequence, turbocharged engines achieve the power level of larger non-charged engines. Smaller engines also exhibit less friction and acceleration losses, which again increases their efficiency compared to larger engines. In addition, a so-called exhaust-gas recirculation (EGR) is often used to lower nitrogen oxide (NOx) emissions [4]. Thereby, the heat capacity of the cylinder charge is increased by the larger molecules of the exhaust gas, leading to a significant reduction of NOx generation. Note that due to its negative effect on the generated engine torque, EGR is only active if required by legislation.

In order to overcome the major disadvantage of exhaust-driven turbochargers, i.e. the lack of boost pressure at low engine speeds, the air system being considered is equipped with two turbochargers (see Figure 1): one designed for the use at low engine speeds and one at high engine speeds. Hence, the system of interest is a two-stage turbocharged system with cooled EGR and charge-air cooling (CAC) as depicted in Figure 1, whose working principle is as follows. Fresh air is aspirated and compressed by the low-pressure compressor (LPC) and further compressed by the high-pressure compressor (HPC), where a by-pass (HPCB) is used in regions of high engine speed and torque. Fresh air cooled by the CAC is mixed with exhaust gas from the EGR in the intake manifold (IM) and then induced into the cylinders. A certain amount of exhaust gas from the exhaust manifold (EM) is recirculated. The remaining exhaust gas drives the high- and low-pressure turbines (HPT and LPT, respectively), which in turn power the compressors. By-passes, i.e. HPTB and LPTB (see Figure 1), are used to control the mass flows through the turbines and consequently the power supplied to the compressors. Note that the high-pressure stage consisting of the HPT, the HPC, and the corresponding connecting shaft HPS, see Figure 1, is designed to be operated at low engine speeds and the respective low-pressure stage is used at high engine speeds. The burned gas finally leaves the air system through the exhaust aftertreatment (EAT).

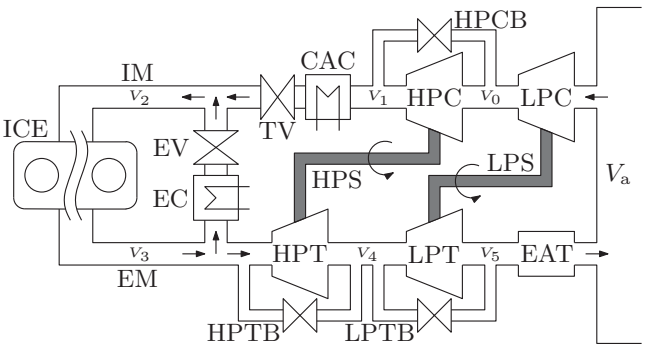

Figure 1: Sketch of the air system with high- and low-pressure compressor (HPC and LPC), charge air cooler (CAC), internal combustion engine (ICE), high- and low-pressure turbine (HPT and LPT), as well as EGR cooler (EC), EGR valve (EV) and the exhaust aftertreatment (EAT).

The purpose of the presented diesel engine air system model is on the hand to serve as simulation model for controller validation and on the other hand to provide a basis for the controller design. Thereby, the controlled air system variables which have to be adjusted in order to realize a desired combustion behavior are the pressure and the composition of the gas mixture in the IM. The available control inputs are on the one hand the valve actuators of the by-passes HPTB and LPTB at the respective turbines for pressure control. On the other hand, the mass flows through the throttle valve (TV) and the exhaust valve (EV) are adjusted using the corresponding actuators in order to manipulate the composition of the gas mixture in the IM.

Assuming a lumped parameter representation, the continuous-time dynamics of the air system is described by a set of nonlinear ordinary differential equations (ODEs) for the respective thermodynamical states in the plenum chambers, i.e. the piping sections (V_0-V_5 in Figure 1) of the air system, as well as for the two turbocharger speeds. Furthermore, the absence and presence of EGR in different operational regions of the engine as well as the employed turbocharging concept necessitate the consideration of different modes of air system operation. These modes are represented by different discrete states (referred to as locations in the sequel) of a finite state machine [3, 9]. The resulting overall air system model consisting of a finite state machine driving the respective underlying continuous-time dynamics is therefore a so-called hybrid automaton or hybrid system [3, 9]. The hybrid dynamical model of the diesel engine air system is derived in Section 2. Phenomenological models approximating those effects whose exact mathematical description turns out to be too complex as well as the associated parameter identification are presented in Section 3. A simulation study including a comparison with measurement data is shown in Section 4, followed by a summary of the results given in the conclusion in Section 5.

2 Hybrid Air System Model

From a modeling perspective, the air system is composed of the engine, the turbochargers, the EAT system, various coolers and valves, as well as the respective interconnecting piping sections V_i, $i=0,\ldots,5$. In the sequel, V_i refers to the i-th plenum chamber. Since the basic mathematical model is the same for all chambers V_i, a modular approach is utilized as described in Section 2.1. Thereby, so-called coupling models, i.e. algebraic descriptions of e.g. the engine or the turbochargers, determine the mass and enthalpy flows between two adjacent chambers. The models of the elements in the modularized air system representation, i.e. plenum chamber and coupling models, are derived in Section 2.2. Finally, the various operational modes together with the switching events occurring during air system operation are represented as locations and transitions of a discrete state machine in Section 2.3.

2.1 Modular Modeling Concept and Basic Assumptions

It is assumed that the spatially distributed piping sections V_i, $i=0,\ldots,5$ of the air system in Figure 1 can be approximated by the lumped parameter model of an ideally mixed plenum chamber as described in Section 2.2.1. The overall model of the air system is then set up in a modularized manner, as can be inferred from the flowsheet of the air system depicted in Figure 2, leading to a set of nonlinear ODEs for the respective thermodynamic states of the plenum chambers. In Figure 2, the dynamical plenum chamber models are interconnected using the algebraic models of e.g. the diesel engine, coolers, or orifices, which are discussed in Sections 2.2.3-2.2.5. For the derivation of both, plenum chamber and coupling models, the gas mixture is supposed to behave like an ideal gas. In particular, the ideal gas law and Dalton's law of partial pressures are assumed to hold, see, e.g. [1].

In Figure 2 the control inputs, i.e. the duty cycles of the actuators for the control valves, are denoted by u_{TV}, u_{EV}, u_{HPTB}, and u_{LPTB}, respectively. It can further be seen that a coupling model determines the mass flow between the two adjacent chambers as well as the temperature of that mass flow. The enthalpy flow into or out of a chamber is then computed by the chamber model on the basis of the provided mass flow and temperature information.

In addition to the continuous-time dynamics, the air system behavior is influenced by different switching events occurring during air system operation. On the one hand, the HPCB (i.e. a check valve) opens if the pressure in chamber V_0 is larger than in V_1. As a consequence, the mass flow through the HPC cannot be used for boost pressure control in this case, resulting in a significantly changed control problem. On the other hand, closing the EV, i.e. deactivating EGR, removes the mass reflux from the exhaust path to the fresh-air path. Both events strongly influence the air system's behavior as discussed in Section 2.3.

2.2 Component Models

On the basis of their ability to store mass and/or energy, the component models are divided into two groups: storage models (i.e. plenum chambers and turbocharger shafts) and coupling models (e.g. orifices, turbines, or the engine). Within the storage models, the general plenum chamber model derived in Section 2.2.1 is a thermodynamical element, while the turbocharger shaft presented in Section 2.2.2 is a mechanical element. The diesel engine model is discussed in Section 2.2.3, followed by the cooler model given in Section 2.2.4. Further coupling models are deduced from the generic orifice model presented in Section 2.2.5.

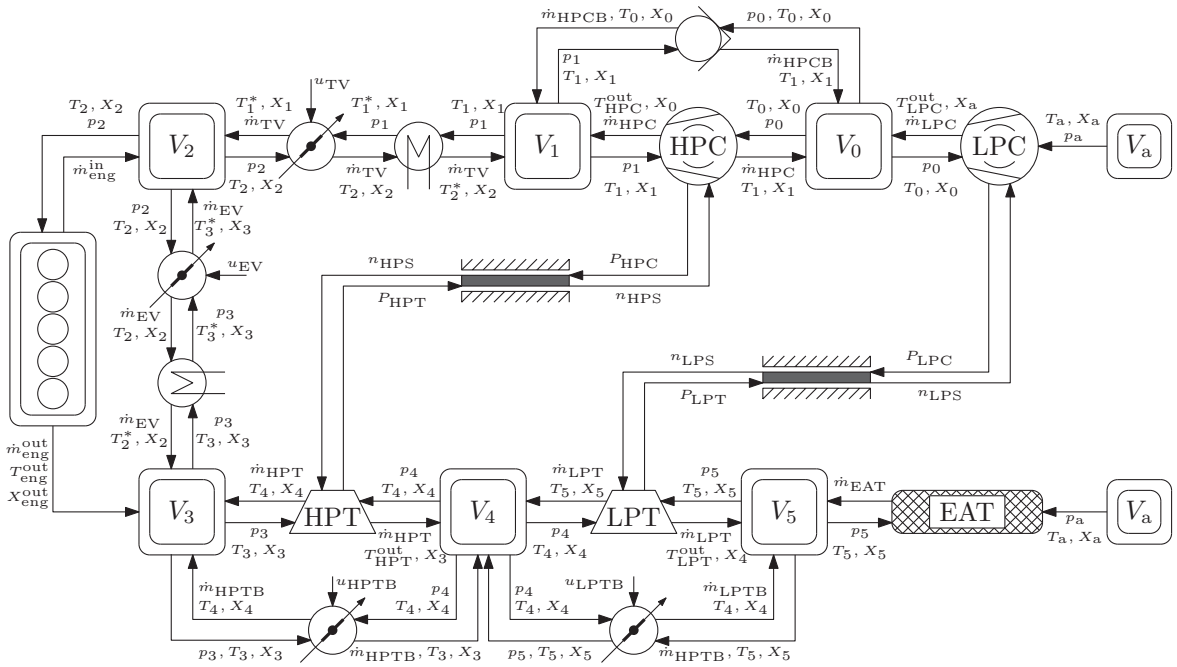

Figure 2: Flow-sheet of the two-stage turbocharged diesel engine air system showing the plenum chambers V_0-V_5, the corresponding algebraic coupling models (diesel engine, valves, compressors, turbines, and exhaust aftertreatment), as well as the interconnecting signals.

2.2.1 Plenum Chambers

In this section, mass and energy balances are used to derive the mathematical model of a general plenum chamber V, which is used as a prototype for the description of the air chambers V_0-V_5. For the set-up of the respective dynamical model, the choice of state variables represents a certain degree of freedom. In order to correctly model the effect of the EGR, i.e. the change of the composition in the IM, the independent variables chosen in this paper are the component masses $m^{(k)}$ and the total pressure p. The respective nonlinear ODEs are given by the corresponding component mass balances and by the total energy balance. In detail, the utilized pressure differential equation is derived from the respective temperature ODE using the ideal gas law, while the temperature ODE is in turn deduced from the energy balance as given by the first law of thermodynamics and the definition of the internal energy. Thereby, the consideration of temperature-dependent gas parameters such as the isochoric and isobaric heat capacities $c_\mathrm{v}(T)$ and $c_\mathrm{p}(T)$, see, e.g. [7], require a definition of the internal energy differing from the well-known caloric relations [1], which typically assume c_v and c_p to be constant.

Mass Balances. The mass balance for a plenum chamber V with N_p physical ports reads as

$$\frac{dm}{dt} = \sum_{i=1}^{N_\mathrm{p}} \dot{m}_i, \tag{1}$$

where m is the total mass stored in the chamber and $\dot{m}_i$ is the mass flow through the i-th port. Throughout this paper, incoming mass flows are positive and outgoing mass flows are negative. Applying the mass balance (1) to each component of the mixture yields the component mass balances

$$\frac{dm^{(k)}}{dt} = \sum_{i=1}^{N_\mathrm{p}} \dot{m}_i^{(k)}, \quad k = 1,\ldots,N^\mathrm{k}, \tag{2}$$

with the mass flow $\dot{m}_i^{(k)}$ of component k through port i and the number of components N_k. The total mass in the chamber is further determined by the sum of all component masses, i.e. $m = \sum_{k=1}^{N_\mathrm{k}} m^{(k)}$. The mass fractions of the components in the chamber are given by $X^{(k)} = \frac{1}{m} m^{(k)}$, $k = 1,\ldots,N_\mathrm{k}$.

Internal Energy. The definition of the internal energy of the gas mixture is used to deduce a temperature ODE from the chamber's energy balance. It is derived on the basis of the total derivative of the internal energy which for pure ideal gases yields [1]

$$du = \frac{\partial u}{\partial T} dT = c_\mathrm{v}(T)dT \quad \Rightarrow \quad \int_{u_0}^{u} d\bar{u} = \int_{T_0}^{T} c_\mathrm{v}(\bar{T})d\bar{T}. \tag{3}$$

From (3), the specific internal energy and accordingly the specific enthalpy are derived in the form

$$u(T) = u_0 + C_\mathrm{v}(T) - C_\mathrm{v}(T_0) \quad \text{and} \quad h(T) = h_0 + C_\mathrm{p}(T) - C_\mathrm{p}(T_0), \tag{4}$$

where $C_\mathrm{v}(T)$ and $C_\mathrm{p}(T)$ are the antiderivatives of the isochoric heat capacity $c_\mathrm{v}(T)$ and the isobaric heat capacity $c_\mathrm{p}(T)$, respectively.

Energy Balance. The energy balance for the plenum chamber with constant volume V is given by the first law of thermodynamics, which for a general resting control volume reads as [1]

$$\frac{dU}{dt} = \dot{Q} + \sum_{k=1}^{N_\mathrm{k}} \sum_{i=1}^{N_\mathrm{p}} \dot{H}_i^{(k)}, \tag{5}$$

where $\dot{Q}$ is the heat transfer through the walls of the chamber and $\dot{H}_i^{(k)} = \dot{m}_i^{(k)} h^{(k)}(\tilde{T}_i)$ denotes the enthalpy flow associated with the mass flow $\dot{m}_i^{(k)}$. The temperature $\tilde{T}_i$ of the mass flow $\dot{m}_i$ is defined as

$$\tilde{T}_i = \begin{cases} T & \text{if} \quad \dot{m}_i < 0, \\ T_i^\mathrm{in} & \text{if} \quad \dot{m}_i \geq 0, \end{cases} \tag{6}$$

with the temperature T_i^in of an incoming mass flow $\dot{m}_i > 0$. Neglecting the heat transfer $\dot{Q}$, Eq. (5) is simplified to

$$\frac{dU}{dt} = \sum_{k=1}^{N_\mathrm{k}} \sum_{i=1}^{N_\mathrm{p}} \dot{m}_i^{(k)} h^{(k)}(\tilde{T}_i). \tag{7}$$

Temperature Differential Equation. With the total internal energy $U = \sum_{k=1}^{N_\mathrm{k}} m^{(k)} u^{(k)}(T)$ stored in the plenum chamber V, the derivative of the internal energy with respect to time amounts with (2) and (4) to

$$\frac{dU}{dt} = \sum_{k=1}^{N_\mathrm{k}} \frac{d(m^{(k)} u^{(k)}(T))}{dt} = \sum_{k=1}^{N_\mathrm{k}} \left(\frac{du^{(k)}(T)}{dt} m^{(k)} + \frac{dm^{(k)}}{dt} u^{(k)}(T) \right) = \sum_{k=1}^{N_\mathrm{k}} \left(m^{(k)} c_\mathrm{v}^{(k)}(T) \frac{dT}{dt} + \sum_{i=1}^{N_\mathrm{p}} \dot{m}_i^{(k)} u^{(k)}(T) \right),$$

which is combined with (7) and solved for the time derivative of the temperature in the chamber to obtain (after some reformulation)

$$\frac{dT}{dt} = \frac{1}{m c_\mathrm{v}(T)} \left(\sum_{k=1}^{N_\mathrm{k}} \sum_{i=1}^{N_\mathrm{p}} \dot{m}_i^{(k)} \left(C_\mathrm{p}^{(k)}(\tilde{T}_i) - C_\mathrm{p}^{(k)}(T) + R^{(k)} T \right) \right), \tag{8}$$

where $R^{(k)}$ is the individual gas constant of component k, $C_\mathrm{p}^{(k)}(T)$ is the antiderivative of the respective isobaric component heat capacity $c_\mathrm{p}^{(k)}(T)$, and $c_\mathrm{v}(T) = \frac{1}{m} \sum_{k=1}^{N_\mathrm{k}} m^{(k)} c_\mathrm{v}^{(k)}(T)$ is the temperature-dependent isochoric heat capacity of the gas mixture in the chamber.

Pressure Differential Equation. The governing differential equation for the total pressure in the plenum chamber is derived using the ideal gas law $pV = mRT$ [1] together with (2), (4), and (8) and amounts to

$$\frac{dp}{dt} = \frac{1}{V} \left((\kappa(T) - 1) \left(\sum_{k=1}^{N_\mathrm{k}} \sum_{i=1}^{N_\mathrm{p}} \dot{m}_i^{(k)} \left(C_\mathrm{p}^{(k)}(\tilde{T}_i) - C_\mathrm{p}^{(k)}(T) \right) \right) + \kappa(T) \sum_{k=1}^{N_\mathrm{k}} \sum_{i=1}^{N_\mathrm{p}} \dot{m}_i^{(k)} R^{(k)} T \right). \tag{9}$$

Thereby, $\kappa(T) = \frac{1}{m} \sum_{k=1}^{N_\mathrm{k}} m^{(k)} \kappa^{(k)}(T)$ is the temperature-dependent isentropic exponent of the gas mixture, with the temperature-dependent isentropic exponents $\kappa^{(k)}(T)$, $k = 1, \ldots, N_\mathrm{k}$, of the gas components.

2.2.2 Turbocharger Shafts

The turbocharger shafts, i.e. the connections between the turbines and compressors, are modeled as rotational masses with an associated moment of inertia J. Viscous friction damping proportional to the shaft's rotational speed ω is assumed. On the basis of the balance of angular momentum, the differential equation for the rotational speed is given by

$$\dot{\omega} = \frac{1}{J} \left(\mathscr{T}_\mathrm{T} + \mathscr{T}_\mathrm{C} - D_\mathrm{f} \omega \right), \tag{10}$$

where $\mathscr{T}_\mathrm{T}$ and $\mathscr{T}_\mathrm{C}$ are the torques generated by the turbine and the compressor, respectively, and $D_\mathrm{f} > 0$ is the friction damping coefficient of the bearing.

2.2.3 Diesel Engine

The engine aspirates fresh-air from the IM (cf. Figures 1 and 2), burns it with diesel fuel, and exhales exhaust gas into the EM. In this work, the engine is described by a so-called mean-value model [4], i.e. a volumetric pump neglecting its crank-shaft driven cyclic behavior. With the density $\rho = \frac{p}{RT}$ of the gas at the intake, the mass flows into and out of the engine can be described by [8]

$$\dot{m}_{\text{eng}}^{\text{in}} = \rho V_{\text{eng}} \frac{n_{\text{eng}}}{2} \eta_{\text{a}} \quad \text{and} \quad \dot{m}_{\text{eng}}^{\text{out}} = \dot{m}_{\text{eng}}^{\text{in}} + \dot{m}_{\text{f}}. \tag{11}$$

Thereby, V_{eng} and n_{eng} are the engine's displacement volume and rotational speed, respectively, and the factor $\frac{1}{2}$ respects the four-stroke cycle of the engine. The variable η_{a} is the so-called air efficiency, describing which part of the maximum possible air mass is actually aspirated by the engine, and $\dot{m}_{\text{f}}$ is the injected fuel mass flow. Assuming that the fuel mass flow $\dot{m}_{\text{f}}$ is burned completely, the composition of the outgoing mass flow $\dot{m}_{\text{eng}}^{\text{out}}$ is determined by the composition of the incoming mass flow $\dot{m}_{\text{eng}}^{\text{in}}$ and the combustion process and can be derived from the chemical reaction equation [6]. Furthermore, the temperature of the exhaust mass flow can be described by

$$T_{\text{eng}}^{\text{out}} = T_{\text{eng}}^{\text{in}} + \Delta T_{\text{c}}, \tag{12}$$

where $T_{\text{eng}}^{\text{in}}$ is the temperature at the engine's inlet and ΔT_{c} is the temperature increase due to combustion. Note that both, the air efficiency η_{a} and the temperature difference ΔT_{c}, depend in general on various parameters, including the engine's speed and load. The respective phenomenological approaches used in this work are discussed in Section 3.1.

2.2.4 Coolers

In the air system, coolers are on the one hand used to reduce the temperature of the charged fresh-air mass flow and on the other hand to reduce the temperature of the recirculated exhaust gas. EGR and charge-air coolers increase the engine's efficiency considerably [4]. Assuming that coolers only affect the mass flow's temperature, i.e. neglecting their fluid-dynamical resistance, they are described by [8]

$$p_{\text{out}} = p_{\text{in}} \quad \text{and} \quad T_{\text{out}} = T_{\text{in}} + \eta_{\text{cool}} \left(T_{\text{cool}} - T_{\text{in}} \right). \tag{13}$$

The cooler efficiency η_{cool} is identified using measurement data, while the coolant temperature T_{cool} is usually known for ECs and CACs. Furthermore, coolers do not change the passing mass flow's composition.

2.2.5 Orifice-Like Elements

As mentioned before, the mass flows through all coupling elements except for the engine and the coolers are described on the basis of an orifice model, i.e. a generic throttling device. Assuming a subsonic isentropic process, the mass flow $\dot{m}$ through the orifice can be derived on the basis of the continuity equation and the first law of thermodynamics, leading to [2]

$$\dot{m} = A p_{\text{in}} \sqrt{\frac{2}{R T_{\text{in}}}} \sqrt{\frac{\kappa}{\kappa - 1} \left(\Pi^{-\frac{2}{\kappa}} - \Pi^{-\frac{\kappa+1}{\kappa}} \right)}, \tag{14}$$

with the cross-sectional area A of the orifice, the isentropic exponent κ, the individual gas constant R, the inlet temperature T_{in}, the pressure ratio $\Pi = \frac{p_{\text{in}}}{p_{\text{out}}}$, and the pressures p_{in} and p_{out} at the in- and outlet, respectively. Most of the considered physical components, however, do not exactly behave like ideal isentropic orifices, i.e. the mass flows predicted by (14) differ from measured mass flows. Therefore, a more general approach, which is well-known in the framework of turbocharger modeling [8], is used. Thereby, the respective mass flow is described using the ansatz

$$\dot{m} = \frac{p_{\text{in}}}{\sqrt{T_{\text{in}}}} \dot{m}^{\text{red}}(\Pi, \mathscr{P}), \tag{15}$$

with the so-called reduced mass flow $\dot{m}^{\text{red}}(\Pi, \mathscr{P})$. The vector $\mathscr{P}$ may contain any time-varying parameters of the device of interest, e.g. the adjustable cross-sectional area of a control valve or a turbine's rotational speed. Suitable phenomenological approaches for the coupling elements of the air system are discussed in Section 3.

2.3 Finite State Machine

Due to their significant influence on the air system's dynamic behavior, different modes of operation have to be distinguished. Thereby, the operational mode is on the one hand determined by the state of the HPCB, i.e. *open* or *closed*, and on the other hand by the EGR status, which can be *on* or *off*. While the HPCB switches its state due to physical effects, i.e. the change of sign of the respective pressure drop at the HPC, the EGR status is adjusted by the control scheme on the basis of the current engine speed and load. This is due to the fact that EGR is only used in a certain subset of the engine's region of operation.

According to [9], a finite state machine can be described by a triple (L,A,E), where L is the finite state space of locations associated with the automaton and A is the respective finite alphabet, whose elements are referred to as symbols. The set $E \subseteq L \times A \times L$ is the corresponding transition rule, whose elements are called edges. With $\{l_i, a_i, l_{i+1}\} \in E, i = 0,\ldots,n-1$, a sequence $\{l_0, a_0, l_1, a_1, \ldots, l_{n-1}, a_{n-1}, l_n\}$ is called a trajectory on the space of locations L [9]. With this formalism, the finite set of possible locations, i.e. operational modes, of the air system is given by

$$L = \{l^1 = (\mathit{closed}, \mathit{on}),\ l^2 = (\mathit{open}, \mathit{on}),\ l^3 = (\mathit{closed}, \mathit{off}),\ l^4 = (\mathit{open}, \mathit{off})\}, \quad (16)$$

where the two entries of l^i refer to HPCB and EGR, cf. Figure 3. The corresponding alphabet [9], i.e. the set of symbols used to label the respective edges, reads as

$$A = \{a^1 = \Delta p_{\mathrm{HPC}} < 0,\ a^2 = \Delta p_{\mathrm{HPC}} \geq 0,\ a^3 = \mathscr{P}_{\mathrm{eng}} \in \Omega_{\mathrm{EGR}},\ a^4 = \mathscr{P}_{\mathrm{eng}} \notin \Omega_{\mathrm{EGR}}\}, \quad (17)$$

where $\Delta p_{\mathrm{HPC}} < (\geq) 0$ means that the pressure difference at the HPC becomes negative (positive), and $\mathscr{P}_{\mathrm{eng}} \in (\notin)\, \Omega_{\mathrm{EGR}}$ describes whether the engine's operating point $\mathscr{P}_{\mathrm{eng}} := (n_{\mathrm{eng}}, \dot{m}_{\mathrm{f}})^T$ is within the region of active EGR or not. Note that the resulting set of events E is restricted to physically meaningful elements of $L \times A \times L$, which is straight-forward and therefore not further discussed here.

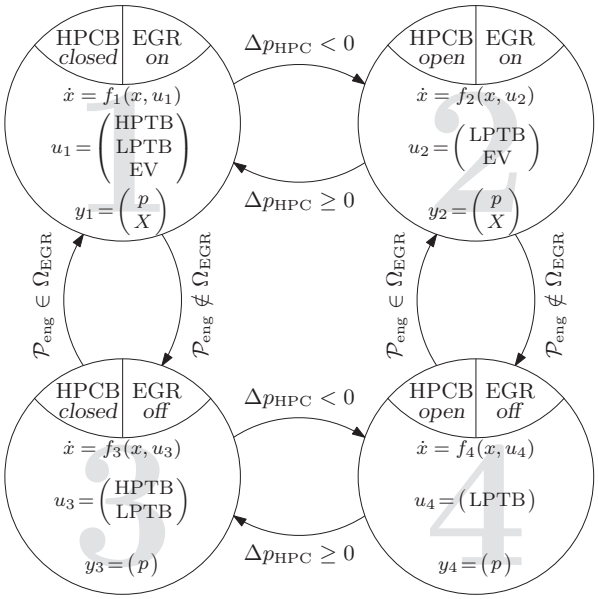

Figure 3: Graph of the automaton for the diesel engine air system with locations l_1-l_4 (marked by light gray numbers within the vertices) and transitions represented by the graph's edges. A set of ODEs as well as respective in- and outputs are associated with each vertice (see inscriptions).

The graph related to the automaton of the air system is depicted in Figure 3. The respective vertices are defined by the elements of L due to (16) and the composition of E can be inferred from the graph's edges, which in turn are labeled by the elements of A due to (17). A nonlinear ODE model is associated with every location. There, it can further be seen that the control problem, especially the dimensions of the control input u and the controlled output y, depends on the location as well.

3 Phenomenological Models and Parameter Identification

A model serving as both, simulation model for controller validation and basis for the controller design, has to be a trade-off between accuracy and complexity. Therefore, certain effects are described phenomenologically instead of using physical laws. Consequently, the coupling element models presented in Section 2.2 comprise phenomenological parameters, such as the engine's air efficiency η_{a}, cf. (11) or reduced mass flows $\dot{m}_{\mathrm{red}}$ through orifice-like elements according to (15). The determination of these quantities as functions of available data, e.g. pressures or speeds, is an important modeling step. The approaches being chosen as well as the respective parameter identification results are exemplarily shown for the diesel engine in Section 3.1, for the EAT in Section 3.2, and for the TV in Section 3.3. Note that throughout this paper, simulation results are given in normalized coordinates, i.e. 0 is the minimum and 1 the maximum of the respective variable, and that the injected fuel mass q_{inj} is used instead of the fuel mass flow $\dot{m}_{\mathrm{f}}$ in addition to the engine speed n_{eng} to define the engine's operating point.

3.1 Diesel Engine

The diesel engine model presented in Section 2.2.3 contains two phenomenological parameters, namely the air efficiency η_{a} and the temperature increase ΔT_{c} caused by combustion. While the air efficiency η_{a} can be described by a linear function of the engine speed, the temperature difference ΔT_{c} turns out to be a function of the engine speed n_{eng} and a weighted ratio of the fuel mass flow $\dot{m}_{\mathrm{f}}$ and the mass flow $\dot{m}_{\mathrm{eng}}^{\mathrm{in}}$ into the engine. In particular, the approaches found to yield excellent results for the diesel engine are

$$\eta_{\mathrm{a}} = a_0 + a_1 n_{\mathrm{eng}} \quad \text{and} \quad \Delta T_{\mathrm{c}} = \underbrace{\frac{H_{\mathrm{i}} \dot{m}_{\mathrm{f}}}{c_{\mathrm{p}}^{\mathrm{air}} \dot{m}_{\mathrm{eng}}^{\mathrm{in}}}}_{=:\Delta T_{\max}} \underbrace{(c_0 + c_1 n_{\mathrm{eng}})}_{=:\eta_{\mathrm{c}}}, \quad (18)$$

where H_{i} is the fuel's inferior heat value and $c_{\mathrm{p}}^{\mathrm{air}}$ is the constant heat capacity of fresh-air at 300 K. Consequently, $\Delta T_{\max}$ is the maximum temperature increase of the fresh-air mass flow $\dot{m}_{\mathrm{eng}}^{\mathrm{in}}$ caused by the combustion of the fuel mass flow $\dot{m}_{\mathrm{f}}$. The factor η_{c} hence defines which part of the maximum temperature increase $\Delta T_{\max}$ of the exhaust gas actually takes place, while the rest of the supplied energy is either used to generate mechanical power or lost

via the cylinder housing. The parameters a_0, a_1, c_0, and c_1 are identified using measurement data, resulting in the parameter curves and approximation errors depicted in Figure 4. Therein, the two left plots show the dependence of η_a and η_c on the engine speed, while the middle and right plots show the approximation errors of the mass flow $\dot{m}_{eng}^{in}$ and the temperature T_{eng}^{out}, respectively.

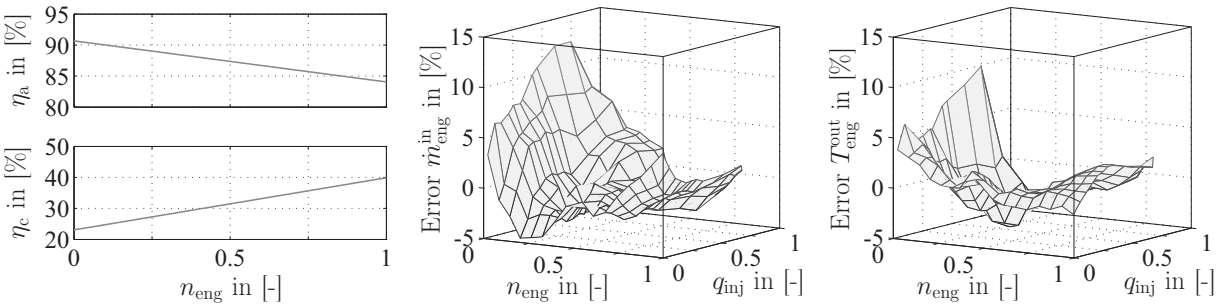

Figure 4: Approximation of the mass flow $\dot{m}_{eng}^{in}$ into the engine and the temperature T_{eng}^{out} of the exhaust gas mass flow $\dot{m}_{eng}^{out}$. Top left: air efficiency η_a. Bottom left: exhaust heating coefficient η_c. Middle: approximation error of the mass flow $\dot{m}_{eng}^{in}$ into the engine. Right: approximation error of the exhaust temperature T_{eng}^{out}.

Figure 4 shows the excellent approximation of the measured mass flow into the engine as well as the temperature of the exhaust gas. Note further that compared to previous approaches [8], the description of the energy used to heat the exhaust gas mass flow given by (18) features improved physical interpretability.

3.2 Exhaust Aftertreatment

Considering only pressure-driven mass flows, the EAT unit generally behaves like an orifice, i.e. it defines the respective mass flow depending on the variables of the attached plenum chambers. However, comparing measurement data and identification results, it turns out that the dependance of the mass flow through the EAT system on the pressure ratio Π cannot be modeled appropriately by the standard approach given by Equation (14), see the left plot in Figure 5. Therefore, the more general approach (15) is chosen, where the respective reduced mass flow $\dot{m}_{EAT}^{red}$ is found to be excellently described by

$$\dot{m}_{EAT}^{red}(\Pi) = a\tanh(b(\Pi-1)^c). \tag{19}$$

The ansatz parameters a, b, and c are identified using measurement data leading to the fit presented in the middle plot of Figure 5. The resulting approximation error with respect to measurements for the mass flow $\dot{m}_{EAT}$ through the EAT utilizing (15) with (19) is depicted in the right plot of Figure 5.

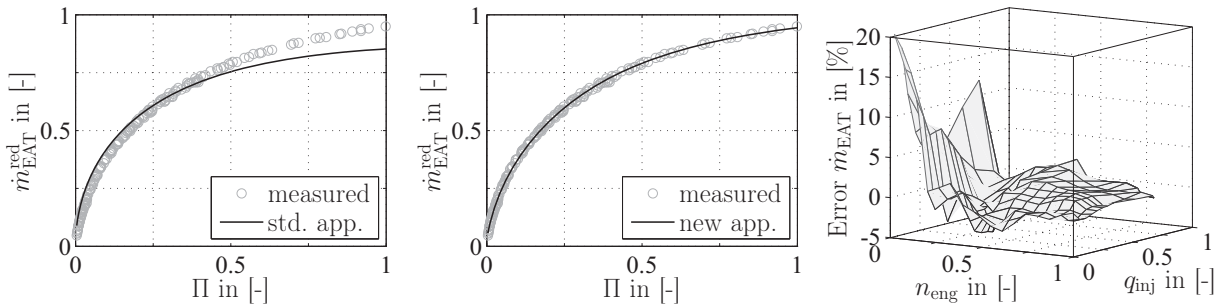

Figure 5: Identification and approximation results for the EAT system. Left: optimal fit of reduced mass flow through EAT using standard approach. Middle: improved fit of reduced mass flow through EAT using adapted ansatz. Right: approximation error of mass flow through EAT system using new approach.

Figure 5 demonstrates the great potential of the ansatz (15) used with a suitable description of the respective reduced mass flow. The reduced mass flow as described by (19) matches the shape of the measured curve better than the standard approach given by (14), while in addition the complexity of the defining equation is reduced.

3.3 Throttle Valve

Similar to the EAT system, the TV's behavior cannot be modeled satisfactorily utilizing the standard approach (14), see dashed line in the left plot of Figure 6. Therefore, as for the EAT system, the more general approach (15) is used to determine the mass flow $\dot{m}_{TV}$ through the TV, with the respective reduced mass flow

$$\dot{m}_{TV}^{red}(\Pi) = \frac{a(\Pi-1)}{1+b(\Pi-1)} \tag{20}$$

leading to the improved fit shown by the solid line in the left plot of Figure 6. Additionally, due to the fact that the TV is a controllable valve, i.e. the mass flow $\dot{m}_{\mathrm{TV}}$ can be adjusted, the corresponding control input u_{TV} has to be included into the TV model. The ansatz (20) is therefore augmented such that it depends on the input u_{TV}. It is found that the input-dependent reduced mass flow $\dot{m}_{\mathrm{TV}}^{\mathrm{red}}$ (cf. Section 2.2.5) can be described by

$$\dot{m}_{\mathrm{TV}}^{\mathrm{red}}(\Pi, u_{\mathrm{TV}}) = \frac{(a_1 - a_2 u_{\mathrm{TV}})(\Pi - 1)}{1 + (b_1 + b_2 u_{\mathrm{TV}})(\Pi - 1)}, \tag{21}$$

where the parameters a_1, a_2, b_1, and b_2 are identified using measurement data. The result of a respective least-squares fit is given in the middle plot of Figure 6, where circles mark the measurement data and crosses mark the respective simulation results. Furthermore, the influence of different values of the control input u_{TV} (i.e. 0%, 25%, 50%, and 75%) on the reduced mass flow $\dot{m}_{\mathrm{TV}}^{\mathrm{red}}$ is shown by the corresponding solid lines. The resulting approximation error of the mass flow $\dot{m}_{\mathrm{TV}}$ through the TV is depicted in the right plot of Figure 6.

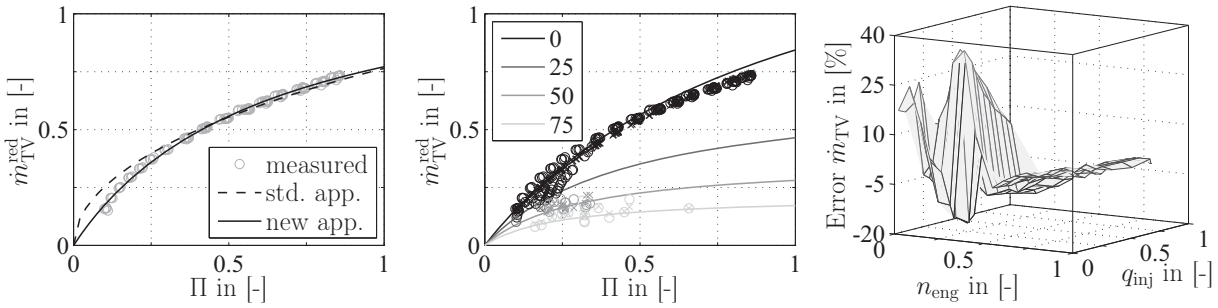

Figure 6: Identification and approximation results for the TV. Left: comparison of standard approach, new approach, and measurement data for fully opened valve. Middle: identified reduced mass flow $\dot{m}_{\mathrm{TV}}^{\mathrm{red}}$ for different values of the control input u_{TV}. Right: approximation error of the mass flow $\dot{m}_{\mathrm{TV}}$ through the TV compared to measurement data.

Although the approximation error of the mass flow $\dot{m}_{\mathrm{TV}}$ through the TV depicted in Figure 6 is larger than those presented before, the achieved results are better than using e.g. the standard approach (14). Thereby, the available data is taken from stationary measurements of the entire engine. Dedicated tests for the TV identification are hence supposed to further improve the results. Note that for further coupling devices, comparable results are achieved. In particular, the speed-dependence of the turbochargers as well as the input-dependence of further valves can be incorporated successfully following the aforedescribed modeling approach.

4 Simulation Results

The qualification of the presented air system model as a simulation model is evaluated in this section. Thereby, stationary simulation results are compared to respective measurement data in Section 4.1. The simulation study presented in Section 4.2 is further used to discuss the dynamic behavior of the air system model.

4.1 Stationary Evaluation of the Air System Model

Interconnecting the presented component models according to the flow-sheet depicted in Figure 2 yields a dynamic model of the air system featuring $n = 20$ states. In order to be suitable for simulation and controller design purposes, the presented air system description has to meet certain accuracy demands. In particular, the correct approximation of the states in the IM and the EM is of major interest. Therefore, the stationary values of the pressure p_2 as well as the temperatures T_2 in the IM and T_3 in the EM are compared to respective measurements in Figure 7. The corresponding approximation error of the aforementioned quantities is shown for all available stationary measurement points.

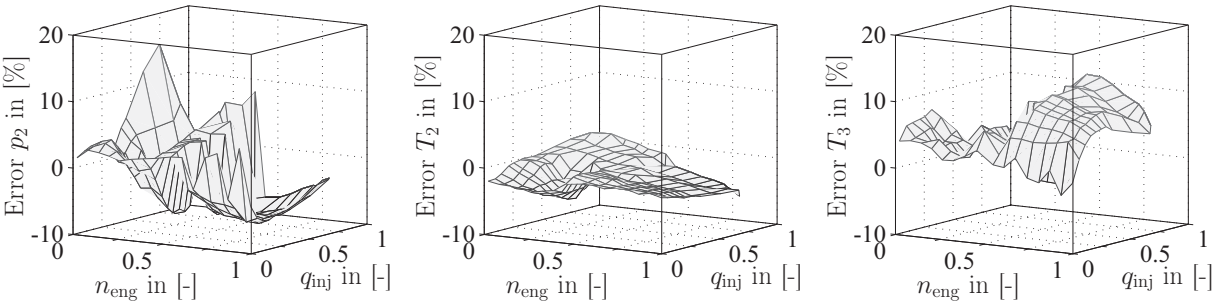

Figure 7: Comparison of stationary simulation and measurement data. Left: pressure p_2 in the IM. Middle: temperature T_2 in the IM. Right: temperature T_3 in the EM.

The approximation errors shown in Figure 7 prove the ability of the presented model to correctly describe the stationary behavior of the diesel engine air system. It is worth mentioning that the approximation errors of further variables are smaller than those shown in Figure 7. Furthermore, it is interesting to notice that throughout the experiments, the temperature approximation is usually closer to measurements than the pressure approximation and that the error plots of the pressures show by far more peaks and lows than the respective plots for the temperatures.

4.2 Dynamic Simulation Results

For the design of model-based (hybrid) controllers, the correct representation of the dynamic behavior is of major importance. In particular, the effects of available inputs and occurring switching events on the plant's behavior are discussed in this section. Due to the lack of respective dynamic measurements, the simulation study presented in Figure 8 intends to demonstrate the effects of different inputs and operating modes on the air system's behavior. There, the chosen input trajectories $u_{\mathrm{TV}}(t)$ (dashed line), $u_{\mathrm{EV}}(t)$ (dash-dotted line), and $u_{\mathrm{HPTB}}(t)$ (solid line) for the actuators of the TV, EV, and HPTB, respectively, are depicted in the top left plot, while the mass flows $\dot{m}_{\mathrm{HPC}}$ through the HPC (dashed line) and $\dot{m}_{\mathrm{HPCB}}$ through the HPCB (solid line) are given in the top right plot. The resulting pressure p_2 (solid line) and temperature T_2 (dashed line) in the IM are shown in the bottom left plot. The mass fractions of oxygen (dashed line) and non-oxygen (solid line) in the IM are given in the bottom right plot. Furthermore, the solid vertical lines mark switching times. In detail, the air system's location changes from l^1 to l^3 at the first vertical line and from l^3 to l^4 at the second. Hence, the trajectory of the discrete state of the air system associated with the presented simulation study reads as $\{l^1, a^4, l^3, a^2, l^4\}$. Note that the engine speed n_{eng} and the injected fuel mass flow $\dot{m}_{\mathrm{f}}$ are constant for the presented simulation results.

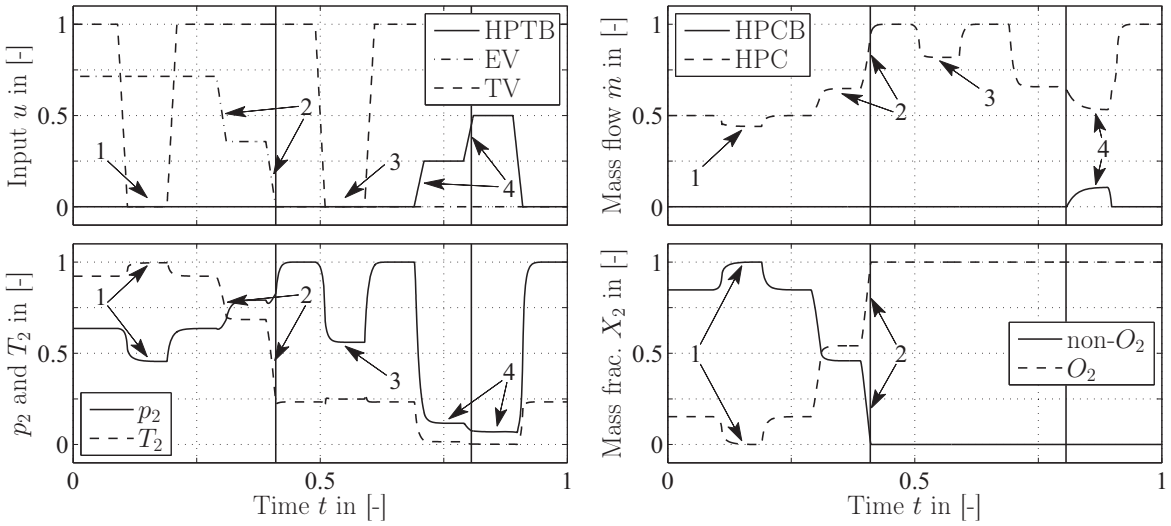

Figure 8: Simulation study showing the effects of control inputs and switching events on the dynamic behavior of the air system. Top left: inputs u_{TV}, u_{EV}, and u_{HPTB}. Top right: mass flows $\dot{m}_{\mathrm{HPC}}$ through HPC and $\dot{m}_{\mathrm{HPCB}}$ through HPCB. Bottom left: resulting pressure p_2 and temperature T_2 in the IM. Bottom right: composition of the mixture in the IM given by the respective mass fractions X_2.

The simulation study presented in Figure 8 features four significant changes of the inputs u_{TV} (1 and 3 in top left plot), u_{EV} (see 2 in Figure 8), and u_{HPTB} (see 4 in Figure 8). Thereby, closing the TV can only affect the composition in the IM if the EV is open, i.e. $u_{\mathrm{EV}} > 0$ (see bottom right plot). Furthermore, closing the TV reduces the mass flow through the HPC (see 1 and 3 in top right plot), which is due to the fact that the consequently decreased mass flow through the air system reduces the power supplied to the HPC. In contrast to the TV, closing the EV increases the mass flow through the turbines and hence the power available for the compressors, leading to an increased mass flow $\dot{m}_{\mathrm{HPC}}$ and boost pressure p_2 (see 2 in top right and bottom left plot). As one expects, the composition of the mixture in the IM is influenced significantly by the EV (see bottom right plot). Finally, the HPTB is opened (see 4 in Figure 8), i.e. the mass flow through the HPT and consequently the power supplied to the HPC is reduced, lowering the mass flow through the HPC (see 4 in the top right plot). As a consequence, the pressure p_2 in the IM drops considerably. The second raise of the HPTB input u_{HPTB} (see 4 in Figure 8) on the one hand further reduces the mass flow $\dot{m}_{\mathrm{HPC}}$ through the HPC, but on the other hand increases the mass flow through the LPC. Therefore, the HPCB opens (i.e. the location of the hybrid dynamical system changes from l_3 to l_4) and the mass flow $\dot{m}_{\mathrm{HPCB}}$ through the compressor bypass is increased (see 4 in the top right plot).

The effects of the control inputs u_{TV}, u_{EV}, and u_{HPTB} can be seen in all plots in Figure 8. The hybrid character of the air system, however, is especially shown by the changed effect of the TV actuation due to the EV closing (compare 1 and 3 in Figure 8) as well as the HPCB opening (see 4 in Figure 8). In fact, closing the EV, in other words changing the location from l_1 to l_3, removes the possibility to influence the mixture in the IM by the TV. Furthermore, the mass flow through the HPCB increases due to the sign change of the pressure drop over the HPC.

5 Conclusion and Outlook

In this contribution, the hybrid model of a two-stage turbocharged diesel engine air system is presented. In particular, plenum chamber models are derived using a temperature-dependent approach, an existing engine model is improved in terms of accuracy and interpretability, and the usefulness of a reduced mass flow approach for the description of throttling elements is proven. Furthermore, switching events and corresponding operational modes of the air system are represented by the edges and vertices of a finite state machine. Stationary measurement results prove the feasibility of the proposed overall mathematical model. In order to further improve the presented model, future research is directed towards dynamic parameter identification, e.g. using the promising technique of combined parameter analysis and identification [5], as well as the generation of respective measurement results. For the design of model-based controllers, a reduced-order description of the air system has to be derived. Thereby, phenomenological approaches as well as systematic techniques can be used to reduce the model complexity. In the context of hybrid control design, the systematic examination of the suitability of different reduced-order models for different operational modes of the air system is an interesting starting point.

6 References

[1] BAEHR, H. D. and S. KABELAC. *Thermodynamik*. Springer Verlag, Berlin, Heidelberg, 13th edition, 2006.

[2] BLACKBURN, J. F., G. REETHOF, and J. L. SHEARER. *Fluid Power Control*. John Wiley & Sons, New York, USA, 1960.

[3] BRANICKY, M. S. *Studies in Hybrid Systems: Modeling, Analysis, and Design*. PhD thesis, Massachusetts Institute of Technology, USA. MIT University Press, Cambridge, 1995.

[4] GUZZELLA, L. and C. H. ONDER. *Introduction to Modeling and Control of Internal Combustion Engine Systems*. Springer Verlag, Berlin, 2004.

[5] MAJER, C. P. *Parameterschätzung, Versuchsplanung und Trajektorienplanung für Verfahrenstechnische Prozesse*. PhD thesis, University of Stuttgart. VDI-Verlag Düsseldorf, Fortschritt-Berichte Reihe 3, Nr. 538, 1998.

[6] MORTIMER, C. E. *Chemie: Das Basiswissen der Chemie*. Thieme Lehrbuchverlag, Stuttgart, 8th edition, 2003.

[7] NATIONAL INSTITUTE OF STANDARDS and TECHNOLOGY. Chemistry WebBook. Available at `http://webbook.nist.gov/chemistry/`.

[8] SCHWARZMANN, D. *Nonlinear Internal Model Control with Automotive Applications*. PhD thesis, Ruhr University Bochum, Germany. Logos Verlag, Berlin, 2007.

[9] VAN DER SCHAFT, A. and H. SCHUMACHER. *An Introduction to Hybrid Dynamical Systems*. Springer Verlag, London, 2000.